

SNS Junctions along the BCS-BEC Crossover

Gautam Rai,¹ Arman Babakhani,² Ying Wang,³ Stephan Haas,^{2,4} and Stefan Kettemann⁴

¹*Institute of Theoretical Physics, University of Hamburg, 22761 Hamburg, Germany*

²*Department of Physics and Astronomy, University of Southern California, Los Angeles, CA 90089-0484, USA*

³*School of Physics and Electronic Engineering, Jiangsu University, Zhenjiang, 212013, PR China*

⁴*Constructor University, Campus Ring 1, 28759 Bremen, Germany*

(Dated: December 2, 2024)

We present a theory of SNS junctions, a normal metal sandwiched between two superconductors, along the crossover from the BCS to the BEC regime. We calculate the Josephson current as a function of the chemical potential relative to the band edge in the superconducting region, μ_S , where the BEC phase is indicated by $\mu_S < 0$. The chemical potential relative to the band edge in the normal metal, μ_N , allows us to tune the junction between the SNS case ($\mu_N > 0$) and the SIS case, where the superconductors are separated by a tunneling barrier. We find that there are Andreev levels in the BEC regime, as long as there is sufficient density of states in the normal region, i.e. when $\mu_N > \Delta$, where Δ is the amplitude of the superconducting order parameter. For 1D SNS junctions, we find the Josephson current I_S carried by these Andreev levels to be a function of the ratio Δ/Δ_d , where Δ_d is the Andreev level spacing. At zero temperature, the Josephson current has a maximum on the BCS side of the transition where Δ is maximal. At finite temperature, however, we find that the maximum moves to the BEC side of the crossover. We identify the mechanism for this phenomenon to be the decrease in the number of Andreev levels at the BCS-BEC crossover, accompanied by an increase in excitation energy to the unoccupied levels, making it less likely that these states are thermally occupied. Thereby, at finite temperature, the Josephson current is more strongly reduced on the BCS side of the crossover, resulting in a maximal Josephson current at the BCS-BEC crossover.

Introduction. Josephson junctions [1] are an excellent platform to study the transport properties of weakly bound Cooper pairs in the BCS regime to tightly bound bosonic pairs in the BEC limit. The Josephson current through an SIS junction, two superconductors separated by a tunnel barrier, is known to exhibit a maximum at the BCS to BEC crossover [2, 3], in agreement with theoretical calculations [4, 5]. SNS junctions, connecting a normal metal with two superconducting leads, have not been considered in the BEC regime so far, even through intriguing questions arise regarding the fate of Andreev levels and the magnitude of the Josephson current in the SNS junction: How many Andreev levels are there in the SNS junction, and is there a maximum in the Josephson current as the Cooper pairs are tuned into tightly bound bosons?

The general theory for the BCS-BEC crossover is well established. Eagles [6] solved BCS equations within a single-band semiconductor model and found a crossover to a BEC condensate as the doping concentration is lowered. The charge carriers form local pairs which condense into a BEC at low temperatures [7]. Nozieres and Pistoletti [8] extended this theory to a two-band model, which was further extended for multi-band systems in Refs. [9–13]. Experimentally, the BCS-BEC crossover was first realized in artificial atom systems [14, 15]. More recently, a BCS-BEC crossover has also been experimentally observed in thin films of Fe-based superconductors [16] by chemical variation of the doping level and in layered nitrides by gate controlled doping [17]. Furthermore, in magic-angle twisted bilayer graphene superconductivity was discovered at low carrier concentrations, tunable by gate controlled doping [18], which opens another venue to investigating the BCS-BEC crossover experimentally. Recently, a novel 1D superconductor was discovered in twisted bilayer graphene [19]. In Ref. [20] a spatial crossover be-

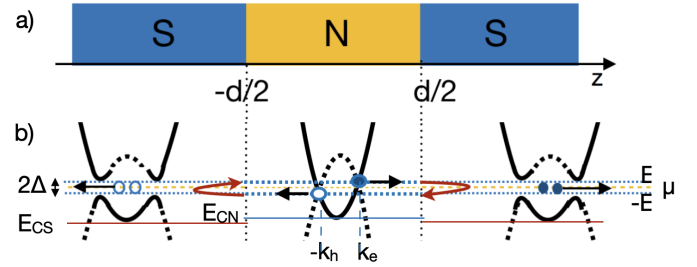


FIG. 1. a) SNS-junction, with a normal region (N) sandwiched between two superconducting leads (S). b) electron and hole dispersions in each region. Blue lines: electron and hole energies relative to the chemical potential μ , E , $-E$. Red arrows: Andreev Scattering of electron with momentum k_e to hole with momentum $-k_h$ and back, forming a clockwise standing wave, an Andreev level. The anticlockwise standing wave, from $-k_e$ to k_h and back, forms another Andreev level (not shown). Red, blue solid lines: band edge in the superconducting, normal region, E_{CS} , E_{CN} , respectively.

tween a BCS and BEC regime was observed by scanning tunneling microscopy in FeSe thin films, deposited on a trilayer graphene substrate. Diminished coherence peaks indicate a normal conduction region, sandwiched between regions in a BCS phase (at a temperature $T < T_C \approx 2K$) and a BEC phase (at $T < T^* \approx 1.4K$), forming an SNS junction.

This motivates us to study SNS-junctions along the BCS-BEC crossover. We aim to derive their properties as a function of the chemical potential relative to the band edge (E_{CS}) in the superconductors, $\mu_S = \mu - E_{CS}$, governing the BCS-BEC crossover. The crossover between SNS and SIS junctions, on the other hand, is governed by the chemical potential $\mu_N = \mu - E_{CN}$, relative to the normal conductor band edge E_{CN} and the thickness of the normal region d , see Fig. 1.

Bogoliubov-De Gennes Equations for SNS Junctions. The

BdG equations for two-component fermionic wave functions are given by [4, 21]

$$\begin{pmatrix} \mathcal{H}(\mathbf{r}) & \Delta(\mathbf{r}) \\ \Delta(\mathbf{r})^* & -\mathcal{H}(\mathbf{r}) \end{pmatrix} \begin{pmatrix} u_n(\mathbf{r}) \\ v_n(\mathbf{r}) \end{pmatrix} = E_n \begin{pmatrix} u_n(\mathbf{r}) \\ v_n(\mathbf{r}) \end{pmatrix}. \quad (1)$$

Here, $\mathcal{H}(\mathbf{r}) = -\nabla^2/(2m) + V(\mathbf{r}) - \mu$, with fermion mass m and external potential $V(\mathbf{r})$. v_n is the probability amplitude that there is a Cooper pair in the state indexed by n , and u_n the amplitude that there is no Cooper pair in that state. The functions $\{u_n(\mathbf{r}), v_n(\mathbf{r})\}$ obey orthonormality conditions. The local order parameter $\Delta(\mathbf{r})$ is determined via the *self-consistency condition* [22] which at $T = 0$ K is given by

$$\Delta(\mathbf{r}) = U \sum_n u_n(\mathbf{r})v_n(\mathbf{r})^*, n(\mathbf{r}) = 2 \sum_n |v_n(\mathbf{r})|^2, \quad (2)$$

where $U > 0$ is the local fermionic attraction strength. The chemical potential μ is determined by the conservation of particle number N , as obtained by integrating the number density $n(\mathbf{r})$ in Eq. (2) over the sample volume, $N = \int d\mathbf{r}n(\mathbf{r})$. In Fig. 1 b), we sketch the local energy dispersions of electrons (solid line) and holes (dashed lines) in the SNS junction. The potential difference between the leads (that become superconducting once the pairing interaction is turned on) and the normal region is given by $V = E_{CS} - E_{CN}$ (see Fig. 1 b)). We distinguish the doping level parameter ϵ , the Fermi energy before the attractive interaction is turned on [8], and μ , the self consistently calculated chemical potential. μ is lowered by the binding energy of the Cooper pairs and is a nonlinear function of the doping level ϵ [8, 23]. We denote $\epsilon_S = \epsilon - E_{CS}$, and $\epsilon_N = \epsilon - E_{CN}$, as the doping levels relative to the conduction band edges in the leads and in the normal region, respectively. The chemical potential μ in the superconducting region is shifted down relative to E_{CS} , lowering $\mu_S = \mu - E_{CS}$ due to the pairing energy in the superconducting condensate. As the doping level ϵ is lowered, one enters the BEC phase in the leads, when the chemical potential drops below the conduction band in the superconductor, that is, when $\mu_S < 0$. The chemical potential relative to the band edge in the normal region μ_N remains constant to ensure charge neutrality. Accordingly, the potential difference between the superconducting and normal region becomes larger $V_{\text{eff}} > V$, due to the pairing energy in the superconducting condensate.

For a bulk superconductor, the quasiparticle energy is given by $E_{\mathbf{k}} = \sqrt{\xi_{\mathbf{k}}^2 + \Delta^2}$, with $\xi_{\mathbf{k}} = \mathbf{k}^2/(2m) - \mu_S$. The density of states of quasiparticle excitations in the BCS regime has a gap 2Δ with two sharp coherence peaks, as sketched in Figs. 3 a) and b). In the BEC phase, $\mu_S < 0$, the energy gap is enlarged to $\Delta_G = \sqrt{\mu_S^2 + \Delta^2} > \Delta$. There, the coherence peaks in the density of states are reduced, and especially the lower one is strongly diminished (see Figs. 3 c) and d)) [20].

The solution of Eq. (1) for an SNS junction is known in the BCS regime: an electron in the normal region with energy $E < \Delta$ forms a standing wave with a hole, with energy $-E$, being reflected at the interface by Andreev scattering, converting the electron into the hole and vice versa,

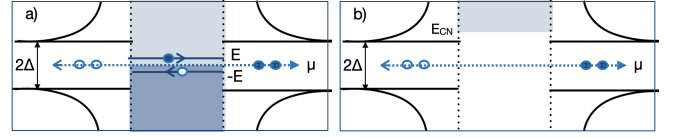


FIG. 2. Schematic density of states of a) BCS-N-BCS junction, b) BCS-I-BCS junction with tunneling barrier $E_{CN} - \mu$.

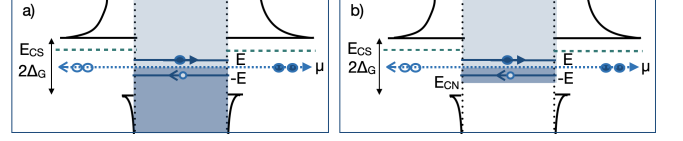


FIG. 3. Schematic density of states of a) BEC-N-BEC junction with $\mu_N = \mu - E_{CN} > \Delta_G$, b) BEC-N-BEC junction with $\mu_N = \mu - E_{CN} < \Delta_G$.

as indicated by the red arrows in Fig. 1 b). The electron and hole amplitudes are for $\{z > d/2, z < -d/2\}$, respectively, given by $\begin{pmatrix} \psi_e(z) \\ \psi_h(z) \end{pmatrix} = \{c_+ \exp(ik_+(z - d/2)) \begin{pmatrix} e^{i\phi_R} \\ e^{-i\varphi_E} \end{pmatrix}, d_+ \exp(ik_-(z + d/2)) \begin{pmatrix} e^{-i\varphi_E} \\ e^{-i\phi_L} \end{pmatrix}\}$, with $\varphi_E = \arccos(E/\Delta)$, $k_+ = (2m(\mu + i\sqrt{\Delta^2 - E^2}))^{1/2}$, $\text{Im}k_+ > 0$ and $k_- = (2m(\mu - i\sqrt{\Delta^2 - E^2}))^{1/2}$, $\text{Im}k_- < 0$. The electron and hole energies are sketched in Fig. 1 b) for the example of a single Andreev bound state in the normal region. The electron moving to the right and the hole moving to the left have equal amplitudes, but different phases ϕ_L, ϕ_R . Next, we match the amplitudes at $z = \pm d/2$ with superpositions of plane waves in the normal region with electron momenta $k_e = (2m(E + \mu_N))^{1/2}$ and hole momenta $k_h = (2m(\mu_N - E))^{1/2}$. We thus obtain the condition for the Andreev level energy, expanding $\Delta k = k_e - k_h$ to first order in E/μ_N for $E \ll \mu_N$, [24–26]

$$\frac{E_n^{+/-}}{\Delta} = \frac{\Delta_d}{\Delta} \left(n + \frac{1}{\pi} \arccos\left(\frac{E_n^+}{\Delta}\right) \pm \frac{\Delta\phi}{2\pi} \right), \quad (3)$$

with the phase difference $\Delta\phi = \phi_R - \phi_L$. Andreev levels close to the center of the gap (where $|E| \ll \Delta$, $\arccos(E/\Delta) \approx \pi/2$) have spacing $\Delta_d = \pi\hbar v_{FN}/d$ with $v_{FN} = \sqrt{2\mu_N}/m$ the Fermi velocity in the normal region. Δ_d is twice the energy level spacing in a 1D normal conductor of length d . The sign \pm corresponds to standing waves with clockwise (+) and anticlockwise (-) Andreev scattering. In Fig. 4, Andreev levels, solutions of Eq. (3), are plotted as a function of the phase difference $\Delta\phi$ and the ratio $\Delta/\Delta_d = d/(\xi\pi)$, proportional to the ratio between length d of the normal metal and the coherence length $\xi = \hbar v_F/\Delta = \pi\xi_0$, where ξ_0 is the Pippard coherence length in the BCS regime.

In the BEC regime, $\mu_S < 0$, we find that Andreev levels still exist as solutions of Eq. (3) for $|E| < \Delta < \Delta_G$, as long as there is sufficient density of states in the normal region, that is $\mu_N > \Delta_d$ and $\Delta_d < \Delta$. For larger energies E , when $\Delta < |E| < \Delta_G$, Andreev and normal scattering mixes. Then, electron and hole amplitudes are no longer equal, so that these

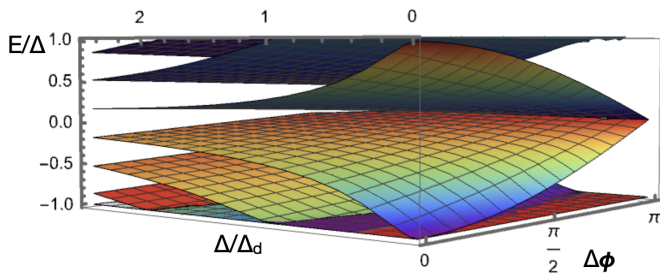


FIG. 4. Andreev levels, Eq. (3), as function of phase difference $\Delta\phi$ and ratio of order parameter and level spacing $\Delta/\Delta_d = d/(\xi\pi)$.

energy levels depend only weakly on the phase difference $\Delta\phi$.

Both in the BCS and BEC regime, the number of Andreev levels is given by $N_A = 2\text{Int}[2\Delta/\Delta_d]$ for $\mu_N > \Delta$. The factor 2 accounts for the pairs of Andreev levels, corresponding to the clockwise and counterclockwise standing waves, Fig. 1. Andreev levels can only form when there is sufficient density of states around the chemical potential in the normal region. This is the case both in the BCS limit, as shown in Fig. 3 a) and in the BEC limit Fig. 3 c), as long as $\mu_N > \Delta$. However, when μ_N is so close to the band edge that $0 < \mu_N < \Delta$, electrons of energy E can only find holes of energy $-E$ in a band of width $2\mu_N < 2\Delta$ around the chemical potential. Then, the number of Andreev states reduces to $N_A = 2\text{Int}[2\mu_N/\Delta_d]$. Inserting $\Delta_d = \hbar v_{\text{FN}}/d$, we find

$$N_A = 2 \begin{cases} \text{Int}\left[\frac{d}{\pi a_0} \frac{\Delta}{\sqrt{\mu_N t}}\right] & \text{for } \Delta < \mu_N, \\ \text{Int}\left[\frac{d}{\pi a_0} \sqrt{\frac{\mu_N}{t}}\right] & \text{for } 0 < \mu_N < \Delta, \end{cases} \quad (4)$$

where $t = \hbar^2/(2ma_0^2)$, and a_0 is the lattice spacing. Note that for a larger number of Andreev levels, their dependence on the phase difference $\Delta\phi$ becomes weaker, as is observed in Fig. 4. For short junctions, when $\Delta_d > \Delta$, Andreev levels cannot form, in which case the junction is in the SIS limit.

Josephson Current. In the BCS regime, the Josephson current through an SIS junction is given by [1, 26]

$$I_s = G_T \pi \frac{\Delta}{e} \sin \Delta\phi, \quad (5)$$

with the tunneling conductance $G_T = G_0 \exp(-2d(2m(V_0 - \mu))^{1/2})$, where $G_0 = 2e^2/h$. It decays exponentially with tunneling barrier width d and height $V_0 - \mu$. In the BCS-BEC crossover regime, the Josephson current through SIS junctions is known to be maximal at the crossover point [4, 5, 27–29], as confirmed experimentally in cold atom systems [2, 3]. This is explained by the fact that the current is limited by the available excitations in the junction. Quasiparticle excitations give an upper limit, which increases when moving from BCS to BEC, while sound wave excitations give a decreasing upper limit when moving from BCS to BEC. This results in a maximal Josephson current at the BCS-BEC crossover [4].

The Josephson current in an SNS junction with a Sharvin

contact is given by [26]

$$I_s = G_N \pi \sum_n f(E_n) \frac{dE_n/e}{d\Delta\phi}, \quad (6)$$

where G_N is the normal state conductance of the junction. A Sharvin contact has a ballistic channel with conductance $G_N = 2e^2/h$. Thus, the Josephson current is carried by occupied Andreev levels $E_n(\Delta\phi)$, Eq. (3), which each contribute a term proportional to their slope in the phase difference $\Delta\phi$. We see in Fig. 4 that subsequent Andreev levels have slopes of opposite sign, so that the current is expected to decrease with the number of occupied Andreev levels. Eq. (6) implies that the Josephson current is mostly carried by occupied Andreev levels, with a small contribution carried by the continuum states located in the energy range outside of the superconductor energy gap, which depends only weakly on $\Delta\phi$. For a more general formulation see Refs. [30, 31, 33].

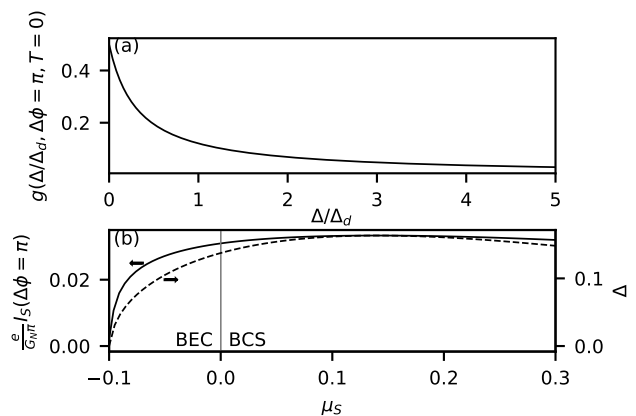


FIG. 5. a) The universal function $g(\Delta/\Delta_d, \Delta\phi = \pi, T = 0)$. b) Order parameter Δ of a 1D superconductor as function of μ_S in units of t , and Josephson current I_s through an SNS junction between 1D superconductors at $T = 0K$ at $\Delta\phi = \pi$ as function of μ_S in units of t . We set $U = 4\pi t/10$, $\mu_N = 0.5t$ and $\Delta_d/t = 1/(2\sqrt{2})$.

According to Eq. (6) the Josephson current is limited by the conductance of the normal metal multiplied by an effective “voltage”, Δ/e , giving the inequality $|I_s| \leq G_N \Delta/e$. Therefore, it is convenient to rewrite Eq. (6) as

$$I_s = G_N \pi \frac{\Delta}{e} g(\Delta/\Delta_d, \Delta\phi, T). \quad (7)$$

$g(\Delta/\Delta_d, \Delta\phi, T)$, is according to Eq. (3) a universal function of the ratio Δ/Δ_d for given $\Delta\phi$ and temperature T . Thus, the Josephson current depends on the junction specific parameters Δ, μ_N, d and the density of states only through the ratio Δ/Δ_d , which also determines the number of Andreev levels N_A , Eq. (4). In Fig 5 a) this function is seen for $\Delta\phi = \pi$ and $T = 0K$ to be a monotonously decaying function of Δ/Δ_d .

We thus identified two opposing mechanisms on the magnitude of the Josephson current in the BCS-BEC crossover

regime: The Josephson current is proportional to 1) the order parameter Δ and 2) a universal function $g(\Delta/\Delta_d, \Delta\phi, T)$, which decreases with the ratio Δ/Δ_d .

Let us consider as an example an SNS junction between 1D superconductors. The density of states of a 1D wire is $\rho(\epsilon_k) = a_0(m/(2\epsilon_k))^{1/2}/\pi$, for $\epsilon_k > 0$. Inserting that into Eq. (2)), we find the order parameter as function of μ_S , shown in Fig. 5 b), with a maximum Δ on the BCS side, $\mu_S > 0$. This maximum is due to the increase of density of states at the band edge in this 1D model, followed by the decrease of Δ when μ_S is tuned into the BEC regime, $\mu_S < 0$. Calculating the contribution of Andreev levels to the Josephson current, Eq. (6), we find that at $T = 0K$ it is a saw tooth function, with maximal amplitude at $\Delta\phi = \pi$, where it jumps to the value with opposite sign. In Fig. 5 b), the amplitude at $\Delta\phi = \pi$ is shown as function of μ_S in units of t . We find a maximal Josephson current amplitude, at a value of μ_S close to the one where the order parameter is maximal.

To calculate the Josephson current at finite temperature $T > 0K$ along the BCS-BEC crossover we insert the Fermi function $f(E_n, T) = 1/(1 + \exp(E_n(\Delta\phi)/T))$ in Eq. (6), with temperature T in units of t . To take into account the temperature dependence of the order parameter, we insert $\Delta(T) = \Delta(0)(1 - 1.76 T/\Delta(0))^{1/2}$, where we used the relation to the mean field critical temperature $T_c = c\Delta(0)$, where $c = 1/1.76$ [22]. We see a decrease with increasing temperature. The jump at $\Delta\phi = \pi$ becomes smooth. In Fig. 6 a), we plot the energy of Andreev levels in units of Δ , as function of phase difference $\Delta\phi$ and chemical potential μ_S . As μ_S moves into the BEC regime, the number of Andreev levels reduces and their dependence on $\Delta\phi$ becomes thereby stronger. At finite temperature, that effects the magnitude of the Josephson effect in another way: the excitation energy to unoccupied Andreev levels increases as μ_S is lowered. Therefore we expect that in the BCS regime, the Josephson current is more diminished with increasing temperature, since the excitation energy to unoccupied Andreev levels, which contribute to the current with an opposite sign, is lower there than in the BEC regime $\mu_S < 0$. Indeed in Fig. 6 b) we see that the maximal Josephson current is located on the BEC side of the crossover, where we plot the Josephson current I_s for temperatures $T = 0.01t$ as function of phase difference $\Delta\phi$ and chemical potential μ_s in units of t . In Fig. 6 c) the maximal (with respect to $\Delta\phi$) Josephson current is plotted as function of μ_S for different temperatures T . We find that the maximum moves to the BEC side of the BCS-BEC crossover as the temperature is increased. In the Supplementary Material, we show results for a system with a band of constant density of states, where we also find a maximal Josephson current, although it remains on the BCS side, close to the BCS-BEC crossover.

Conclusions and Discussion. We have analyzed SNS-junctions along the BCS-BEC crossover regime. We showed that Andreev levels exist as long as there is sufficient density of states in the normal metal. Furthermore, we find a maximum in the Josephson current which moves with increasing temperature into the BEC regime. The mechanism for this

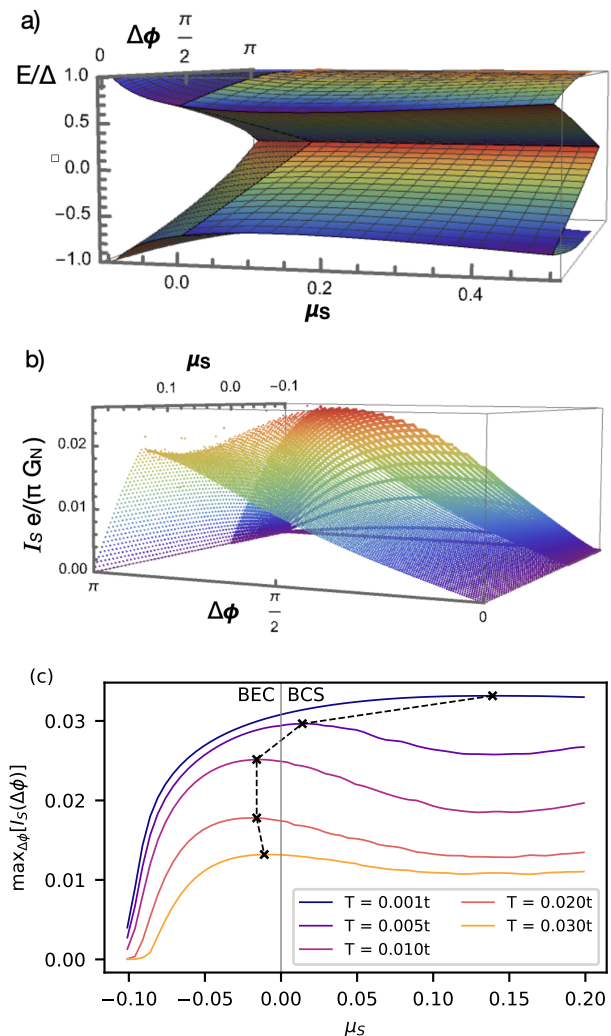


FIG. 6. a) Andreev levels, energy in units of Δ , as function of phase difference $\Delta\phi$ and chemical potential μ_S . b) Josephson current I_s Eq. (6) in 1D SNS-junctions for temperature $T = 0.01t$ as function of phase difference $\Delta\phi$ and chemical potential μ_S . c) The maximal (with respect to $\Delta\phi$) Josephson current as function of μ_S for different temperatures T . The crosses mark the maximum along the BCS-BEC crossover (with respect to μ_S). We set $U = 4\pi t/10$, $\mu_N = 0.5t$ and $\Delta_d/t = 1/(2\sqrt{2})$.

phenomenon is identified as the decrease of the number of Andreev levels at the BCS-BEC crossover with an accompanying increase in excitation energy, thus making thermal excitations less likely on the BEC side. In a forthcoming publication, we will report the results of a numerical analysis of the BdG equations for SNS junctions on a tight-binding model [32].

In Josephson junctions with more than one transverse channels, there is finite angle Andreev scattering, which can be described by semiclassical transport theory, solving the Eilenberger equations [33]. This method also allows to include finite transparency of the junction and disorder scattering which is present in any real sample and may reduce the Josephson current further. In future work, we plan to extend this theory and apply it to the BCS-BEC crossover regime. Furthermore, 1D superconductors are experiencing quantum and thermal

fluctuations, which requires to go beyond the BdG equations, as reviewed in Ref. [34]. To study its effect on the Josephson current, one needs to extend the theory of SNS junctions including the quantum fluctuations in the BCS-BEC crossover regime, which will be the subject of further investigations.

S.K. gratefully acknowledges support from DFG KE-807/22-1. This work was supported by the US Department of Energy under grant number DE-FG03-01ER45908.

-
- [1] B. D. Josephson, *Physics Letters*. **1**, 251 (1962).
- [2] D. E. Miller, J. K. Chin, C. A. Stan, Y. Liu, W. Setiawan, C. Sanner and W. Ketterle *Phys. Rev. Lett.* **99**, 070402 (2007).
- [3] W. Weimer, K. Morgener, V. P. Singh, J. Siegl, K. Hueck, N. Luick, L. Mathey, H. Moritz, *Phys. Rev. Lett.* **114**, 095301 (2015).
- [4] A. Spuntarelli, P. Pieri, G.C. Strinati, *Physics Reports* **488**, 111 (2010).
- [5] M. Zaccanti and W. Zwerger *Phys. Rev. A* **100**, 063601 (2019).
- [6] D. M. Eagles, *Phys. Rev.* **186**, 456 (1969).
- [7] A. J. Leggett, Diatomic molecules and Cooper pairs, in *Modern Trends in the Theory of Condensed Matter*, ed. by A. Perali and Przystawa, Springer, Berlin (1980).
- [8] P. Nozieres and F. Pistolesi, *Eur. Phys. J. B* **10**, 649 (1999).
- [9] X. Chen, S. Maiti, A. Linscheid, and P. J. Hirschfeld, *Phys. Rev. B* **92**, 224514 (2015).
- [10] A. V. Chubukov, I. Eremin, D. V.Efremov, *Phys. Rev. B* **93**, 174516 (2016).
- [11] Y. L. Loh, M. Randeria, N. Trivedi, C.-C. Chang, R. Scalettar, *Phys. Rev. X* **6**, 021029 (2016).
- [12] J. Boeker, P. A. Volkov, K. B. Efetov, I. Eremin, *Phys. Rev. B* **96**, 014517 (2017).
- [13] Y. Yerin, H. Tajima, P. Pieri, A. Perali, *Phys. Rev. B* **100**, 104528 (2019).
- [14] C. A. Regal, M. Greiner, D. S. Jin, *Phys. Rev. Lett.* **92**, 040403 (2004).
- [15] M. W. Zwierlein, C. A. Stan, C. H. Schunck, S. M. F. Raupach, A. J. Kerman, W. Ketterle, *Phys. Rev. Lett.* **2004** **92**, 120403.
- [16] S. Rinott, K. B. Chashka, A. Ribak, E. D. L. Rienks, A. Taleb-Ibrahimi, P. L. Fevre, F. Bertran, M. Randeria, and A. Kanigel. *Science Advances*, **3**(4) (2017).
- [17] Y. Nakagawa, Y. Saito, T. Nojima, K. Inumaru, S. Yamanaka, Y. Kasahara, and Y. Iwasa. *Phys. Rev. B*, **98**:064512 (2018).
- [18] Y. Cao, V. Fatemi, S. Fang, K. Watanabe, T. Taniguchi, E. Kaxiras, and P. Jarillo-Herrero, *Nature (London)* **556**, 43 (2018).
- [19] J. Barrier, M. Kim, R. K. Kumar, N. Xin, P. Kumaravadivel, L. Hague, E. Nguyen, A. I. Berdyugin, C. Mouldsdale, V. V. Enaldiev, J. R. Prance, F. H. L. Koppens, R. V. Gorbachev, K. Watanabe, T. Taniguchi, L. I. Glazman, I. V. Grigorieva, V. I. Fal'ko, A. K. Geim, *Nature* **628**, 741 (2024).
- [20] H. Lin, W. Huang, G. Rai, Y. Yin, L. He, S. Haas, S. Kettemann, X. Chen, S.-H. Ji, *Spectroscopic evidence of BCS-BEC crossover in FeSe monolayer*, *Phys. Rev. B* **107**, 104517 (2023).
- [21] P. G. De Gennes, *Rev. Mod. Phys.* **36**, 225 (1964).
- [22] J. R. Schrieffer, *Theory of Superconductivity*, Perseus Books (1999).
- [23] A. Niroula, G. Rai, S. Haas, S. Kettemann, *Phys. Rev. B* **101**, 094514 (2020).
- [24] A.F. Andreev, *Sov. Phys. JETP* **22**, 455–458 (1966).
- [25] I. G. Kulik, *Zh. Eksp. Teor. Fiz.* **57**, 1745 (1969)[*Sov. Phys. JETP* **30**, 944 (1970)].
- [26] J. A. Sauls, *Philos. Trans. A Math. Phys. Eng. Sci.* **376**(2125), 20180140 (2018).
- [27] F. Setiawan and J. Hofmann *Phys. Rev. Research* **4**, 043087 (2022)
- [28] C. Lewandowski, E. Lantagne-Hurtubise, A. Thomson, S. Nadj-Perge and J. Alicea, *Phys. Rev. B* **107** L020502 (2023).
- [29] F. Pascucci, L. Salasnich, *Phys. Rev. A* **102**, 013325 (2020).
- [30] T. Löfwander, V. S. Shumeiko, G. Wendin, *Superconductor Science and Technology* **14**, R53 (2001).
- [31] T. T. Heikkilä, J. Särkkä and F. K. Wilhelm, *Phys. Rev. B* **66**, 184513 (2002).
- [32] A. Babakhani, G. Rai, Y. Wang, S. Haas, S. Kettemann, *to be submitted*.
- [33] D. Nikolić, W. Belzig, and J. C. Cuevas *Phys. Rev. Research* **1**, 033031 (2019).
- [34] K. Y. Arutyunov, D. S. Golubev, A. D. Zaikin, *Physics Reports* **464**, 1 (2008).